Resonant Magnetization Tunneling in the Trigonal Pyramidal Mn IV Mn III 3 Complex [Mn 4 O 3 Cl(O 2 CCH 3) 3 (dbm) 3]

ARTICLE *in* JOURNAL OF THE AMERICAN CHEMICAL SOCIETY · MAY 1998

Impact Factor: 12.11 · DOI: 10.1021/ja974241r

Resonant Magnetization Tunneling in the Trigonal Pyramidal $Mn^{IV}Mn^{III}_3$ Complex $[Mn_4O_3Cl(O_2CCH_3)_3(dbm)_3]$

Sheila M. J. Aubin,[†] Neil R. Dilley,[‡] Luca Pardi,[§] J. Krzystek,[§] Michael W. Wemple,[⊥] Louis-Claude Brunel,[§] M. Brian Maple,*[,‡] George Christou,*[,⊥] and David N. Hendrickson*[,†]

Contribution from the Department of Chemistry and Biochemistry-0358, University of California at San Diego, La Jolla, California 92093-0358, Department of Physics, University of California at San Diego, La Jolla, California 92093, Center for Interdisciplinary Magnetic Resonance, National High Magnetic Field Laboratory, Florida State University, Tallahassee, Florida, 32310, and Department of Chemistry, Indiana University, Bloomington, Indiana 47405-4001

Received December 15, 1997

Abstract: The trigonal pyramidal complex $[Mn_4O_3Cl(O_2CCH_3)_3(dbm)_3]$, where dbm^- is the monoanion of dibenzoylmethane, functions as a single-molecule magnet. High-field EPR data are presented for an oriented microcrystalline sample to characterize the electronic structure of the $Mn^{IV}Mn^{III}_3$ complex. These data show that the complex has a $S = {}^9/_2$ ground state, experiencing axial zero-field splitting ($D\hat{S}_z^2$) with $D = -0.53$ cm^{-1} and a quartic zero-field splitting ($B_4^0\hat{O}_4^0$)with $B_4^0 = -7.3 \times 10^{-5}$ cm^{-1}. Magnetization versus external magnetic field data were collected for an oriented single crystal in the 0.426−2.21 K range. At temperatures below 0.90 K hysteresis is seen. Steps are seen on each hysteresis loop. This is clear evidence that each $Mn^{IV}Mn^{III}_3$ complex functions as a single-molecule magnet that is magnetizable. Furthermore, the steps on the hysteresis loops are due to resonant magnetization quantum mechanical tunneling. In response to an external field each molecule reverses its direction of magnetization not only by being thermally activated over a potential-energy barrier, but by the magnetization tunneling through the barrier. Additional evidence for resonant magnetization tunneling was found in the change in the temperature at which the out-of-phase ac magnetic susceptibility is observed as a function of an external dc field. The results of magnetization relaxation experiments carried out in the 0.394−0.700 K range are presented. These data are combined with the ac susceptibility data taken at higher temperatures to give an Arrhenius plot of the logarithm of the magnetization relaxation rate versus inverse absolute temperature. The temperature-dependent part of this plot gives an activation barrier of 11.8 K. Below 0.6 K the relaxation rate is independent of temperature with a rate of 3.2 $\times 10^{-2}$ s^{-1}. This $S = {}^9/_2$ single-molecule magnet exhibits a tunneling of its direction of magnetization at a rate of 3.2 $\times 10^{-2}$ s^{-1} in the 0.394−0.600 K range. Thus, resonant magnetization tunneling is seen for a half-integer-spin ($S = {}^9/_2$) ground-state magnet in the absence of an external magnetic field. The transverse component of the small magnetic field from the nuclear spins is probably the origin of this tunneling.

Introduction

The unusual magnetic properties of single-molecule magnets have been the focus of considerable research. A single-molecule magnet is a molecule that has an appreciable potential-energy barrier for reversal of the direction of its magnetic moment. The barrier results from a high-spin ground state exhibiting significant magnetic anisotropy. Large negative magnetic anisotropy ($D\hat{S}_z^2$) is experienced by each molecule as a result of axial zero-field splitting of a high-spin ground state. At low temperatures the spins of the molecules sluggishly flip from "up" to "down" along the magnetic anisotropy axis and therefore slow magnetic relaxation is observed. Single-molecule magnets are of interest for several reasons. First, they display magnetic properties such as slow magnetic relaxation and quantum-mechanical tunneling as studied in macroscopic iron oxide single domain particles (1−100 nm), where the magnetic response is due to long-range ordering of spins. Considerable research is directed at studying single-molecule magnets in order to elucidate how quantum-mechanical behavior observed in these molecules underlies classical behavior at the macroscopic scale.[1] Second, the miniaturization of magnetic technology as well as the rapid growth of high-speed computers has fueled research in the field of nanoscale magnetic materials.[2] Since each molecule could store one bit of information and a typical molecule size is 10 Å, large amounts of information could be stored.

At present only a few single-molecule magnets are known. Taft et al.[3] and Papaefthymiou[4] employed Mössbauer spectros-

[†] Department of Chemistry and Biochemistry-0358, University of California at San Diego.
[‡] Department of Physics, University of California at San Diego.
[§] Florida State University.
[⊥] Indiana University.

(1) (a) Awschalom, D. D.; Di Vincenzo, D. P. *Phys. Today* **1995**, *48*, 43. (b) Leslie-Pelecky, D. L.; Rieke, R. D. *Chem. Mater.* **1996**, *8*, 1770. (c) Gunther, L. *Phys. World* **1990**, December 28. (d) Awschalom, D. D.; Di Vincenzo, D. P.; Smyth, J. F. *Science* **1992**, *258*, 414. (e) Stamp, P. C. E.; Chudnosvsky, E. M.; Barbara, B. *Int. J. Mod. Phys.* **1992**, *B6*, 1355. (f) Gider, S.; Awschalom, D. D.; Douglas, T.; Mann, S.; Chaparala, M. *Science* **1995**, *268*, 77.
(2) Dahlberg, E. D.; Zhu, J.-G *Phys. Today* **1995**, 34.
(3) Taft, K. L.; Papaefthymiou, G. C.; Lippard, S. J. *Science* **1993**, *259*, 1302.

S0002-7863(97)04241-8 CCC: $15.00
Published on Web 05/07/1998

copy to demonstrate the superparamagnetic behavior of Fe_{12} and $Fe_{16}Mn$ molecular complexes. One family of single-molecule magnets is $[Mn_{12}O_{12}(O_2CR)_{16}(H_2O)_x]$, where R is CH_3 (**1**)[5−33] with $x = 4$, R is Et (**2**)[34−38] with $x = 3$ and R is Ph (**3**)[39−41] with $x = 4$. An $[Mn_{12}]^-$ salt, $PPh_4[Mn_{12}O_{12}(O_2CEt)_{16}(H_2O)_4]$ (**4**), has also been reported to be a single-molecule magnet.[34−38] All of these Mn_{12} complexes exhibit magnetic hysteresis loops. A second family of Mn clusters with a $[Mn^{IV}Mn^{III}{}_3O_3X]^{6+}$ core has been reported to display frequency-dependent out-of-phase magnetic susceptibility peaks, a property indicative of the slow magnetic relaxation of single-molecule magnets.[42−44] Finally, Barra *et al.*[45] have reported that the ferric complex $[Fe_8O_2(OH)_{12}(tacn)_6]^{8+}$ (**5**), where tacn is triazacyclononane, functions as a single-molecule magnet based on slow magnetic relaxation observed in ac susceptibility and Mössbauer studies.

Of all these single-molecule magnets, $[Mn_{12}O_{12}(O_2CCH_3)_{16}(H_2O)_4]\cdot 4H_2O\cdot 2HO_2CCH_3$ (**1**), also referred to as Mn_{12}-Ac, is the most thoroughly studied. Recently resonant magnetization tunneling has been observed for Mn_{12}Ac (**1**)[18−20] a Mn_4 complex,[42b] and Fe_8 (**5**).[46] Steps were observed at regular intervals of magnetic field in the magnetization hysteresis loops for oriented-crystal samples. The observed steps in the hysteresis loop correspond to an increase in the rate of decrease of magnetization occurring when there is alignment of energy levels in the two halves of the potential-energy plot for a single-molecule magnet. In addition, a temperature-independent rate of relaxation was observed[46] below 0.400 K for the Fe_8 complex **5**.

In this paper, evidence of resonant magnetization tunneling is presented for a third single-molecule magnet, $[Mn_4O_3Cl(O_2CCH_3)_3(dbm)_3]$ (**6**), where dbm^- is the monoanion of dibenzoylmethane. Previously, complex **6** was reported[42] to have a well-isolated $S = {}^9/_2$ ground state that is split by axial zero-field splitting, $|D| \sim 0.4$ cm^{-1}. Frequency-dependent out-of-phase ac susceptibility peaks were reported for a microcrystalline sample of complex **6**, indicating slow magnetic relaxation. Out-of-phase ac susceptibility signals were also seen for a frozen solution of complex **6**. Therefore, the origin of the slow magnetization relaxation was deduced to be single-molecule anisotropy, rather than long-range ordering of the spins of molecules. In this paper, high-field EPR data are presented for complex **6** that confirm the magnetic anisotropy in this system. Considerable data are presented to conclusively establish that complex **6** is a single-molecule magnet. Furthermore, definitive hysteresis loop and magnetization relaxation data are also presented to show that this half-integer-spin molecule exhibits quantum mechanical tunneling of the direction of its magnetization.

(4) Papaefthymiou, G. C. *Phys. Rev.* **1992**, *B46*, 10366.
(5) Lis, T. *Acta Crystallogr*. **1980**, *B36*, 2042.
(6) Caneschi, A.; Gatteschi, D.; Sessoli, R.; Barra, A. L.; Brunel, L. C.; Guillot, M. *J. Am. Chem. Soc*. **1991**, *113*, 5873.
(7) Sessoli, R.; Gatteschi, D.; Caneschi, A.; Novak, M. A. *Nature* **1993**, *365*, 141.
(8) Gatteschi, D.; Caneschi, A.; Pardi, L.; Sessoli, R. *Science* **1994**, *265*, 1054.
(9) Villain, J.; Hartman-Boutron, F.; Sessoli, R.; Rettori, A. *Europhys. Lett*. **1994**, *27*, 159.
(10) Barra, A. L.; Caneschi, A.; Gatteschi, D.; Sessoli, R. *J. Am. Chem. Soc*. **1995**, *117*, 8855.
(11) Novak, M. A.; Sessoli, R.; Caneschi, A.; Gatteschi, D. *J. Magn. Magn. Mater*. **1995**, *146*, 211.
(12) Barbara, B.; Wernsdorfer, W.; Sampaio, L. C.; Park, J. G.; Paulsen, C.; Novak, M. A.; Ferré, R.; Mailly, D.; Sessoli, R.; Caneschi, A.; Hasselbach, K.; Benoit, A.; Thomas, L. *J. Magn. Magn. Mater*. **1995**, *140*−*144*, 1825.
(13) Novak, M. A.; Sessoli, R. In *Quantum Tunneling of Magnetization-QTM′94*; Gunter, L., Barbara, B., Eds.; Kluwer Academic Publishers: Dordrecht, 1995; pp 171−188.
(14) Paulsen, C.; Park, J.-G. In *Quantum Tunneling of Magnetization-QTM′94*; Gunther, L., Barbara, B., Eds.; Kluwer Academic Publishers: Dordreht, 1995; pp 189−207.
(15) Paulsen, C.; Park, J.-G.; Barbara, B.; Sessoli, R.; Caneschi, A. *J. Magn. Magn. Mater*. **1995**, *140*−*144*, 379.
(16) Paulsen, C.; Park, J. G.; Barbara, B.; Sessoli, R.; Caneschi, A. *J. Magn. Magn. Mater*. **1995**, *140*−*144*, 1891.
(17) Politi, R.; Rettori, A.; Hartmann-Boutron, F.; Villain, J. *Phys. Rev. Lett*. **1995**, *75*, 537.
(18) Friedman, J. R.; Sarachik, M. P.; Tejada, J.; Maciejewski, J.; Ziolo, R. *J. Appl. Phys*. **1996**, *79*, 6031.
(19) (a) Friedman, J. R.; Sarachik, M. P.; Tejada, J.; Ziolo, R. *Phys. Rev. Lett*. **1996**, *76*, 3830. (b) Friedman, J. R. Ph.D. Thesis 1996, The City College of New York, New York City, NY.
(20) Thomas, L.; Lionti, F.; Ballou, R.; Gatteschi, D.; Sessoli, R.; Barbara, B. *Nature* **1996**, *383*, 145.
(21) Tejada, J.; Ziolo, R. F.; Zhang, X. X. *Chem. Mater*. **1996**, *8*, 1784.
(22) Hernandez, J. M.; Zhang, X. X.; Luis, F.; Bartolomé, J.; Tehadra, J.; Ziolo, R. *Europhys. Lett*. **1996**, *35*, 301.
(23) Chudnovsky, E. M. *Science* **1996**, *274*, 938.
(24) Reynolds, P. A.; Gilbert, E. P.; Figgis, B. N. *Inorg. Chem*. **1996**, *35*, 545.
(25) Gatteschi, D. *Curr. Opin. Solid State Mater. Sci*. **1996**, *1*, 192.
(26) Burin, A. L.; Prokof'ev, N. V.; Stamp, P. C. E. *Phys. Rev. Lett*. **1996**, *76*, 3040.
(27) Politi, P.; Rettori, A.; Harmann-Boutron, F.; Villain, J. *Phys. Rev. Lett*. **1996**, *76*, 3041.
(28) Schwarzschild, B. *Phys. Today* **1997**, January 17.
(29) Lionti, F.; Thomas, L.; Ballou, R.; Barbara, B.; Sulpice, A.; Sessoli, R.; Gatteschi, D. *J. Appl. Phys*. **1997**, *81*, 4608.
(30) Friedman, J. R.; Sarachik, M. P.; Hernandez, J. M.; Zhang, X. X.; Tejada, J.; Molins, E.; Ziolo, R. *J. Appl. Phys*. **1997**, *81*, 3978.
(31) Barra, A. L.; Gatteschi, D.; Sessoli, R. *Phys. Rev. B* **1997**, *56*, 8192.
(32) Luis, F.; Bartolomé, J.; Fernández, J. F. *Phys. Rev. B* **1997**, *55*, 11448.
(33) Hernandez, J. M.; Zhang, X. X.; Luis, F.; Tejada, J.; Friedman, J. R.; Sarachik, M. P.; Ziolo, R. *Phys. Rev. B* **1997**, *55*, 5858.
(34) Eppley, J. J.; Tsai, H.-L.; De Vries, N.; Folting, K.; Christou, G.; Hendrickson, D. N. *J. Am. Chem. Soc*. **1995**, *117*, 301.
(35) Eppley, J. J.; Wang, S.; Tsai, H.-L.; Aubin, S. M.; Folting, K.; Streib, W. E.; Hendrickson, D. N.; Christou, G. *Mol. Cryst. Liq. Cryst*. **1995**, *274*, 159.
(36) Tsai, H.-L.; Eppley, J. J.; de Vries, N.; Folting, K.; Christou, G.; Hendrickson, D. N. *Mol. Cryst. Liq. Cryst*. **1995**, *274*, 167.
(37) Aubin, S. M. J.; Spagna, S.; Eppley, H. J.; Sager, R. E.; Folting, K.; Christou, G.; Hendrickson, D. N. *Mol. Cryst. Liq. Cryst*. **1997**, *305*, 181.
(38) Eppley, H. J.; Aubin, S. M. J.; Wemple, M. W.; Adams, D. M.; Tsai, H.-L.; Grillo, V. A.; Castro, S. L.; Sun, Z.; Folting, K.; Huffman, J. C.; Hendrickson, D. N.; Christou, G. *Mol. Cryst. Liq. Cryst*. **1997**, *305*, 167.
(39) Boyd, P. D. W.; Li, Q.; Vincent, J. B.; Folting, K.; Chang, H.-R.; Streib, W. E.; Huffman, J. C.; Christou, G.; Hendrickson, D. N. *J. Am. Chem. Soc*. **1988**, *110*, 8537.
(40) Schake, A. R.; Tsai, H.-L.; de Vries, N.; Webb, R. J.; Folting, K.; Hendrickson, D. N.; Christou, G. *J. Chem. Soc., Chem. Commun*. **1992**, 181.
(41) Sessoli, R.; Tsai, H.-L.; Schake, A. R.; Wang, S.; Vincent, J. B.; Folting, K.; Gatteschi, D.; Christou, G.; Hendrickson, D. N. *J. Am. Chem. Soc*. **1993**, *115*, 1804.
(42) (a) Aubin, S. M. J.; Wemple, M. W.; Adams, D. M.; Tsai, H.-L.; Christou, G.; Hendrickson, D. N. *J. Am. Chem. Soc*. **1996**, *118*, 7746. (b) Aubin, S. M. J.; Dilley, N. R.; Wemple, M. W.; Maple, M. B.; Christou, G.; Hendrickson, D. N. *J. Am. Chem. Soc*. **1998**, *120*, 839.
(43) (a) Hendrickson, D. N.; Christou, G.; Schmitt, E. A.; Libby, E.; Bashkin, J. S.; Wang, S.; Tsai, H.-L.; Vincent, J. B.; Boyd, P. D. W.; Huffman, J. C.; Folting, K.; Li, Q.; Streib, W. E. *J. Am. Chem. Soc*. **1992**, *114*, 2455. (b) Wemple, M. W.; Adams, D. M.; Folting, K.; Hendrickson, D. N.; Christou, G. *J. Am. Chem. Soc*. **1995**, *117*, 7275. (c) Wemple, M. W.; Adams, D. M.; Hagen, K. S.; Folting, K.; Hendrickson, D. N.; Christou, G. *J. Chem. Soc., Chem. Commun*. **1995**, 1591. (d) Wang, S.; Folting, K.; Streib, W. E.; Schmitt, E. A.; McCusker, J. K.; Hendrickson, D. N.; Christou, G. *Angew. Chem., Int. Ed. Engl*. **1991**, *30*, 305. (e) Wang, S.; Tsai, H.-L.; Streib, W. E.; Christou, G.; Hendrickson, D. N. *J. Chem. Soc., Chem. Commun*. **1992**, 1427. (f) Wang, S.; Tsai, H.-L.; Libby, E.; Folting, K.; Streib, W. E.; Hendrickson, D. N.; Christou, G. *Inorg. Chem*., **1996**, *35*, 7578.
(44) Wemple, M. W.; Tsai, H.-L.; Folting, K.; Hendrickson, D. N.; Christou, G. *Inorg. Chem*. **1993**, *32*, 2025.
(45) Barra, A.-L.; Debrunner, P.; Gatteschi, D.; Schulz, Ch. E.; Sessoli, R. *Europhys. Lett*. **1996**, *35*, 133.
(46) Sangregorio, C.; Ohm, T.; Paulsen, C.; Sessoli, R.; Gatteschi, D. *Phys. Rev. Lett*. **1997**, *78*, 4645.

Experimental Section

Sample Preparation. An analytically pure sample of [$Mn_4O_3Cl(O_2CCH_3)_3(dbm)_3$], complex **6**, was prepared according to the literature method.[43d,f]

Physical Measurements. Magnetization data were collected on a Faraday magnetometer equipped with a ^{3}He cryostat capable of achieving temperatures as low as 0.35 K. The operating field range is −50 to 50 kOe. Alternating current (ac) magnetic susceptibility experiments were carried out on a Quantum Design MPMS2 SQUID magnetometer equipped with a 10 kOe magnet. The ac field strength can be varied from 0.001 to 5 Oe at frequencies ranging from 0.0005 to 1512 Hz. The temperature can be varied from 1.7 to 400 K.

Magnetization hysteresis loops were measured on an oriented single crystal (63 μg) of [$Mn_4O_3Cl(O_2CCH_3)_3(dbm)_3$] (**6**). The crystal was first added to eicosane (12 mg) and aligned in a 55 kOe field. The temperature was then raised above the melting point of eicosane (312−318 K), held there for 20 min, and then reduced to room temperature to set. The resulting wax cube contained one crystal oriented such that the axial magnetic anisotropy (easy) axis of the molecule is parallel to the applied magnetic field. Hysteresis measurements were carried out on the resulting oriented crystal in the temperature range 0.4 to 2.2 K, while sweeping the field from 20 to −20 kOe and back to 20 kOe.

Ac magnetic susceptibility measurements were made on oriented microcrystals (14.4 mg) of [$Mn_4O_3Cl(O_2CCH_3)_3(dbm)_3$] (**6**). The microcrystals were aligned in a 55.0 kOe field and set in eicosane as described above. Ac susceptibility data were measured as a function of temperature at different settings of a dc field. The ac field amplitude was 1 Oe, oscillating at a frequency of 1000 Hz.

High-field EPR spectra were recorded for [$Mn_4O_3Cl(O_2CCH_3)_3(dbm)_3$] (**6**) at the National High Magnetic Field Laboratory, located at Florida State University. The high-field EPR spectrometer is capable of achieving fields up to 14.5 T in the temperature range of 2−300 K and is equipped with several sources for generating radiation in the millimeter and sub-millimeter range. In this work, a Gunn diode operating at a fundamental frequency of 110 ± 3 GHz was used. The operating frequency range is 110 to 550 GHz. Frequencies between 220 and 550 GHz were obtained by using a solid-state harmonic generator that multiplies the fundamental frequency (*i.e.*, 110 GHz) and high pass filters to filter out the lower frequency harmonics. For example, if a 220 GHz filter is used, the 110 GHz component is blocked, but the higher harmonic frequencies (e.g., 330, 440 GHz, etc.) pass through.[48] A modulation frequency of 8.00 kHz and a modulation amplitude of 2.5 mT were used. The field was swept at a rate of 0.5 T/min in the 0 to 13 T range and 0.3 T/min in the 13 to 14.5 T range. A microcrystalline sample was studied. Because of the large external field and the sample's predisposition to orient in a field, the resulting EPR data are pseudo-single-crystal spectra. That is, all of the small crystallites in the sample were aligned in the large field and only the $g_{\parallel}$ EPR spectrum is observed. The magnetic field was calibrated by adding a small amount of DPPH to the sample. Data were also collected on a powdered sample of complex **6** that was pressed into a pellet to prevent the crystallites from rotating in the applied magnetic field.

Results and Discussion

High-Field EPR Measurements. The single-crystal X-ray structure of complex **6** has been reported.[43d,f] Complex **6** crystallizes in the monoclinic $P2_1/n$ space group with $Z = 4$. The molecule has the trigonal pyramidal $[Mn^{IV}Mn^{III}_3O_3Cl]^{6+}$ core pictured below. A C_3 symmetry axis runs through the Mn^{IV} and Cl atoms and defines the magnetic *z*-axis of each molecule. The four molecules within a unit cell are canted at an angle of 8.97° with respect to one another. Magnetic susceptibility data have established that the spin of the ground state is $S = {}^9/_2$,

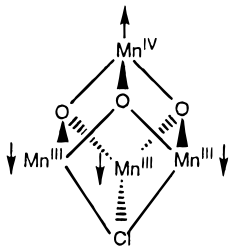

where the $Mn^{IV}\cdots Mn^{III}$ interactions are antiferromagnetic ($J = -23.4$ cm^{-1}) and the $Mn^{III}\cdots Mn^{III}$ interactions are ferromagnetic ($J = 8.3$ cm^{-1}). The dominant antiferromagnetic $Mn^{IV}\cdots Mn^{III}$-exchange interactions force the spins on the Mn^{III} ions to be antiparallel to the spin on the Mn^{IV} ion. The $S = {}^9/_2$ ground state is very well isolated with the lowest energy excited state at 180 cm^{-1} higher energy.[43f] Large magnetic anisotropy was evident from fitting of magnetization data collected on a microcrystalline sample. Since the Mn atoms are exchange coupled in **6**, the axial single-ion zero-field interactions ($D\hat{S}_z^2$) present at each Mn^{III} ion give rise to an axial zero-field splitting for the $S = {}^9/_2$ ground state of the molecule. The variable-field magnetization data for **6** could be equally well fit[43f] with either a positive *D* parameter ($D = +0.45$ cm^{-1}) or a negative one ($D = -0.35$ cm^{-1}). The sign of the *D* parameter is definitively determined in this work.

High-field EPR (HFEPR) spectra were taken for [$Mn_4O_3Cl(O_2CCH_3)_3(dbm)_3$] (**6**) that unequivocally confirm that the sign of *D* is negative. Unlike magnetic susceptibility data that are a bulk property reflecting a Boltzmann population of states, direct transitions between states are seen in an EPR experiment. Changes in relative intensities of EPR peaks reflect changes in Boltzmann populations and can be used to directly determine the sign of *D*. An X-band (9 GHz) EPR spectrum has been reported[43f] previously for a frozen toluene glass of complex **6**. At 5 K, three broad signals are seen at $g = 1.96$, 5.2, and 11.0. At higher temperatures, the signals became even broader. This X-band spectrum is difficult to interpret because complex **6** has a high-spin $S = {}^9/_2$ ground state and $|D| \simeq 0.4$ cm^{-1} which is close to the energy of the X-band EPR frequency.

The obvious advantage of HFEPR (110−550 GHz) in probing molecules with large-spin ground states is that more transitions are seen and therefore the HFEPR spectra are considerably more informative. Fine structure, that is, a series of relatively constantly spaced transitions, is seen due to the zero-field splitting of the ground state. In principle, the spin of the ground state can be determined by simply counting the number of transitions observed in such a series and dividing by 2. The sign of the zero-field splitting parameter *D* can be determined by observing the temperature dependence of the peaks comprising the fine structure. With inclusion of only axial zero-field splitting, the spin Hamiltonian for a $S = {}^9/_2$ complex can be written[43a] as

$$\hat{H} = g\mu_B \hat{H}\cdot\hat{S} + D[\hat{S}_z^2 - {}^1/_3 S(S+1)] \qquad (1)$$

In the high-field limit where $g\mu_B H_o \gg (2S-1)D$ the spectrum for a $S = {}^9/_2$ complex can be interpreted readily. The resonance field at which an EPR allowed transition from a M_s state to a $(M_s + 1)$ state occurs is given in eq 2,

$$H_r = (g_e/g)[H_o - (2M_s + 1)D'] \qquad (2)$$

where $D' = (3\cos^2\theta - 1)D/(2g_e\mu_B)$ and θ is the angle between the external magnetic field and the anisotropy axis (i.e., the C_3

(47) (a) Loss, D.; DiVincenzo, D. P.; Grinstein, G.; Awschalom, D. D.; Smyth, J. F. *Physica B* **1993,** *189*, 189. (b) Di Vincenzo *Physica B* **1994**, *197*, 109.

(48) Barra, A.-L.; Brunel, L.-C.; Gatteschi, D.; Pardi, L.; Sessoli, R. Submitted for publication.

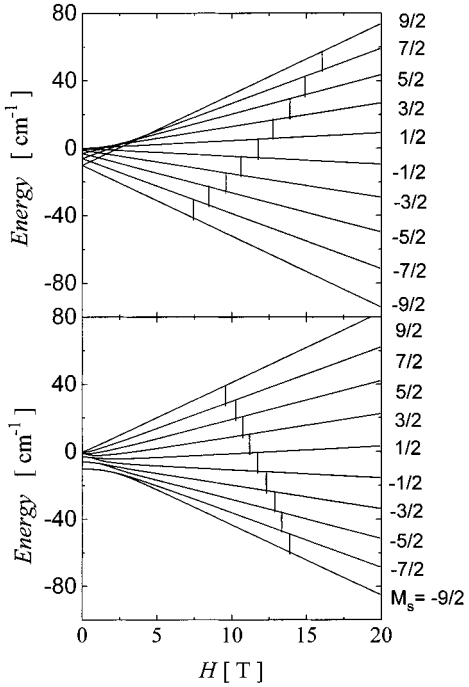

Figure 1. Plot of the energy vs the external magnetic field (H) for the 10 zero-field split components of the $S = {}^9/_2$ ground state. The axial zero-field splitting, $D\hat{S}_z^2$, is characterized by $D = -0.53$ cm^{-1} and $g = 1.998$. In the upper part of the figure, the magnetic field is oriented parallel to the principal axis of magnetic anisotropy, while in the lower part of the figure the magnetic field is oriented perpendicular to the z axis.

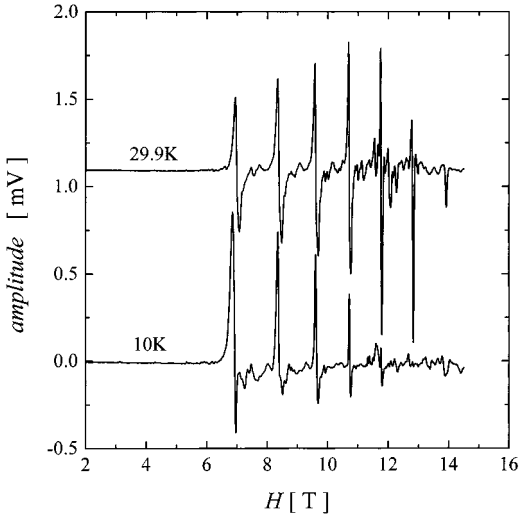

Figure 2. High-field EPR spectra for an oriented microcrystalline sample of complex **6** collected at 327.9 GHz and temperatures of 10 and 30 K.

axis of complex **6**). For the parallel transitions ($\theta = 0°$), the peaks are separated by $2D'$, while for the perpendicular transitions ($\theta = 90°$), a spacing of D' is observed. As shown in Figure 1, when the magnetic field is oriented either parallel or perpendicular to the C_3 axis of complex **6**, nine $\Delta M_s = \pm 1$ allowed transitions are expected. In this figure the energy of each of the zero-field split components of the $S = {}^9/_2$ ground state is plotted as a function of field for the case where $g = 2$ and $D = -0.5$ cm^{-1}. The transitions expected at a frequency of 327 GHz are shown. Clearly, the separations between the parallel transitions are twice those for the perpendicular transitions. Nine parallel transitions will be seen in the EPR sectrum when there are molecules populating all of the states from the lowest energy state with $M_s = -{}^9/_2$ to the highest energy state with $M_s = {}^9/_2$. At low temperature where all of the molecules are in the $M_s = -{}^9/_2$ state, then only the $M_s = -{}^9/_2$ to $M_s = -{}^7/_2$ transition is observed. For a parallel field orientation (Figure 1, top) when $D < 0$, this $-{}^9/_2$ to $-{}^7/_2$ transition is seen at the lowest field position. If $D > 0$ for a $S = {}^9/_2$ complex, then the $-{}^9/_2$ to $-{}^7/_2$ transition occurs at the highest field position in the fine structure series. Thus, by observing the temperature dependence of a series of fine structure peaks, the sign of D can be definitively determined.

HFEPR spectra were recorded for a microcrystalline sample of $[Mn_4O_3Cl(O_2CCH_3)_3(dbm)_3]$ (**6**). Due to the large magnetic anisotropy exhibited by this complex together with the large fields employed, the microcrystals orient in the field and therefore the resulting EPR spectrum is for the case where the easy axis (i.e., axis of largest magnetic susceptibility) of each microcrystal is aligned parallel to the external magnetic field. The net result is that the C_3 axes of individual molecules are canted by 4.49° relative to the direction of the external magnetic field. The magnetic field was calibrated by adding a small amount of diphenyldipicrylhydrazide (DPPH) to the sample. Such quasicrystal spectra were collected for $[Mn_4O_3Cl(O_2CCH_3)_3(dbm)_3]$ (**6**) at several frequencies (218.6, 327.9, and 437.2 GHz) at temperatures of 10 and 30 K. In Figure 2, the spectra taken at 327.9 GHz for complex **6** at temperatures 10 and 30 K are shown. At 10 K, five sharp peaks are seen between 7 and 12 T. Each resonance corresponds to a transition from one $|S,M_s\rangle$ zero-field level to another for the $S = {}^9/_2$ ground state. The resonance at the lowest field corresponds to the transition from the $M_s = -{}^9/_2$ to the $M_s = -{}^7/_2$ state. The resonances that follow, en suite, correspond to the $-{}^7/_2 \rightarrow -{}^5/_2$, $-{}^5/_2 \rightarrow -{}^3/_2$, $-{}^3/_2 \rightarrow -{}^1/_2$ and $-{}^1/_2 \rightarrow {}^1/_2$ transitions, respectively. The relative intensities of the peaks directly reflect the Boltzmann populations of the states. As temperature is increased, higher energy states are populated and therefore additional transitions are observed at *higher* fields. Thus, the spectrum run at 29.9 K (Figure 2) shows seven fine-structure peaks up to the field limit of the spectrometer. It can be concluded that D is negative.

HFEPR spectra collected for a pellet of complex **6** further substantiate that the sign of D is negative. In this case there is a random orientation of molecules relative to the external field direction. The microcrystals were pressed into a pellet. The powder HFEPR spectrum collected at 4.4 K with a frequency of 327.6 GHz is available in the Supporting Information. At 4.4 K, three distinct sets of peaks are seen in the field range of 6.92−9.62 T, a second group of three peaks in the 10.88−12.27 T range, and a third group of three peaks in the 13.8−14.6 T range. The three peaks seen in the 6.92−9.62 T region are the ones seen in the quasicrystal spectra. The separations between the peaks seen in the 6.92−9.62 T region are ∼1.4 T, while the separations are ∼0.7 T for the other two groupings of three peaks. Since the separation between the parallel peaks is expected to be twice as large as the separation between the perpendicular transitions, it can be concluded that the peaks in the 6.92−9.62 T region are the parallel field transitions, while the peaks observed at the higher fields in the powder spectrum are due to the perpendicular transitions.

Quasicrystal EPR spectra for magnetic field aligned microcrystals were also collected at different frequencies and different temperatures. In Figure 3 are shown three spectra recorded at 30 K for frequencies of 218.6, 327.9, and 437.2 GHz. At 218.6 GHz, two sets of signals are seen, one set resulting from a

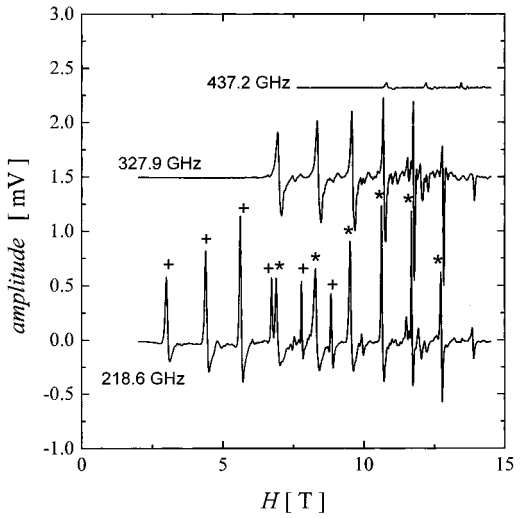

Figure 3. HFEPR spectra for an oriented microcrystalline sample of complex **6** collected at 30 K for frequencies of 218.6, 327.9, and 437.2 GHz. In the spectrum taken at a nominal frequency of 218.6 GHz, transitions due to both 218.6 GHz (+) and 327.9 GHz (*) are also seen.

Table 1. Pseudo Crystal High-Field EPR Transition Fields for [$Mn_4O_3Cl(O_2CCH_3)_3(dbm)_3$] (6) at 218.59 GHz and Temperatures of 29.3 and 9.99 K

	transition field, H [T]			
transitions $M_s \rightarrow M_s + 1$	218.6 GHz, 29 K, H(down)[a]	327.9 GHz,[c] 29 K, H(down)	218.6 GHz, 10 K, H(up)	327.9 GHz,[c] 10 K, H(up)
$-9/2 \rightarrow -7/2$	3.042	6.929	3.054	6.82 (w)[b]
$-7/2 \rightarrow -5/2$	4.434	8.319	4.468	8.36 (w)[b]
$-5/2 \rightarrow -3/2$	5.649	9.542	5.712	9.63 (w)[b]
$-3/2 \rightarrow -1/2$	6.769	10.649	6.821	10.73 (w)[b]
$-1/2 \rightarrow 1/2$	7.807	11.702	7.87	
$1/2 \rightarrow 3/2$	8.867	12.751		
$3/2 \rightarrow 5/2$	9.95 (w)[b]	13.87 (w)[b]		

[a] Direction in which the field was swept: down means the field was swept from high field to zero and up means from zero to high field. [b] (w) means a low intensity peak. [c] Peaks resulting from 327.9 GHz while using the 220 GHz high-pass filter.

microwave frequency of 218.6 GHz (+) and the other set due to the 327.9 GHz (∗) frequency. High pass filters are used to adjust the frequency and block out lower harmonic frequencies, but not higher harmonic frequencies. In comparing the spectra at the different frequencies it is observed that with increasing frequency, the transitions are shifted to higher fields. A complete list of the resonance fields at different temperatures and frequency is available in Tables 1 and 2.

By using the quasicrystal EPR data, the resonance field at which the transitions occur was calculated with eq 2. Since the molecules are canted at 8.98° with respect to each other, the angle θ between the external magnetic field and the z-axis of each molecule is 4.49°. In Figure 4 the resonance fields (H_r) at which transitions are seen are plotted vs $(2M_s + 1)$ for the different temperatures and frequencies at which data were collected. If a $S = 9/2$ ground state is assumed, least-squares fitting of these data to eq 2 leads to a reasonable fit with $g = 2.0$ and $D' = -0.57$ cm^{-1}. Since $\theta = 4.49°$, this gives the value of $D = -0.54$ cm^{-1}. However, the data fall on a curved line, while eq 2 predicts a straight line. The transitions are *not* seen at a constant interval of field. For example, at 327.88 GHz and 29.9 K transitions are observed at 6.99, 8.38, 9.60, 10.7, 11.8, 12.8, and 13.9 T. The corresponding separations between these peaks are, starting at the lowest field, 1.39, 1.22, 1.11, 1.05, 1.04, and 1.08 T. With increasing field, the separation decreases and then begins to increase again.

Table 2. Pseudo Crystal High-Field EPR Transition Fields for [$Mn_4O_3Cl(O_2CCH_3)_3(dbm)_3$] (**6**) at 327.9 and 437.2 GHz

	transition field, H [T]		
transitions $M_s \rightarrow M_s + 1$	327.9 GHz, 30 K, H(up)[a]	327.9 GHz,[b] 10 K, H(up)	437.2 GHz, 30 K, H(down)
$-9/2 \rightarrow -7/2$	6.988	6.918	10.8 (w)
$-7/2 \rightarrow -5/2$	8.383	8.379	12.2 (w)
$-5/2 \rightarrow -3/2$	9.604	9.630	13.4 (w)
$-3/2 \rightarrow -1/2$	10.711	10.735	
$-1/2 \rightarrow 1/2$	11.763	11.78 (w)	
$1/2 \rightarrow 3/2$	12.808		
$3/2 \rightarrow 5/2$	13.89 (w)[b]		

[a] Direction in which the field was swept: down means the field was swept from high field to zero and up means from zero to high field. [b] (w) means a low intensity peak.

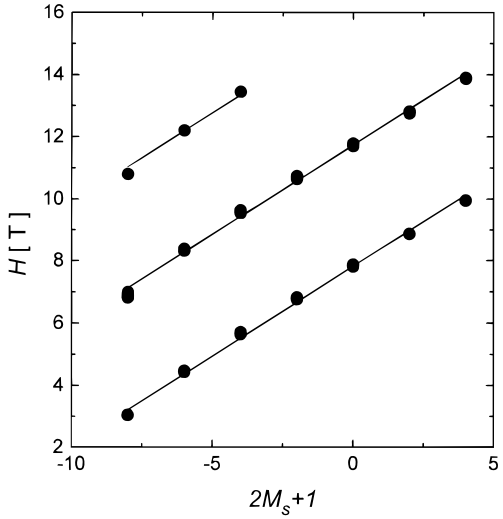

Figure 4. Plot of the resonance fields at which transitions occur plotted versus the value of $(2M_s + 1)$ taken from the pseudo-single-crystal HFEPR data collected for complex **6** at frequencies of 220, 330, and 440 GHz and temperatures of 10 and 30 K. The solid line is a least-squares fitting of these data to eq 2 where $\theta = 0$. The fitting parameters are described in the text.

To accommodate the data, the quartic zero-field interaction term $B_4^0\hat{O}_4^0$ was added to the spin Hamiltonian to give[31] eq 3:

$$\hat{H} = g\mu_B\hat{H}\cdot\hat{S} + D[\hat{S}_z^2 - {}^1/_3S(S+1)] + B_4^0\hat{O}_4^0 \qquad (3)$$

where $\hat{O}_4^0 = 35\hat{S}_z^4 - 30S(S+1)\hat{S}_z^2 + 25\hat{S}_z^2 + 6S(S+1)$. After some algebraic manipulations, the resonance field for a parallel transition from a M_s state to a $(M_s + 1)$ state is expressed as

$$H_r = \frac{g_e}{g}[H_o - (2M_s+1)(D' + 25B_4^{0'} - 30S(S+1)B_4^{0'}) - 35B_4^{0'}(4M_s^3 + 6M_s^2 + 4M_s + 1)] \quad (4)$$

where, $B_4^{0'} = (B_4^0/2g_e\,\mu_B)(3\cos^2\theta - 1)$. Since the ground-state spin is $S = 9/2$, eq 4 can be further simplified to give:

$$H_r = \frac{g_e}{g}[H_o - (2M_s+1)(D' - 717.5B_4^{0'}) - 35B_4^{0'}(4M_s^3 + 6M_s^2 + 4M_s + 1)] \quad (5)$$

The resonance field data obtained at 220, 330, and 440 GHz were least-squares fit to eq 5 to give a very good fit with $g =$

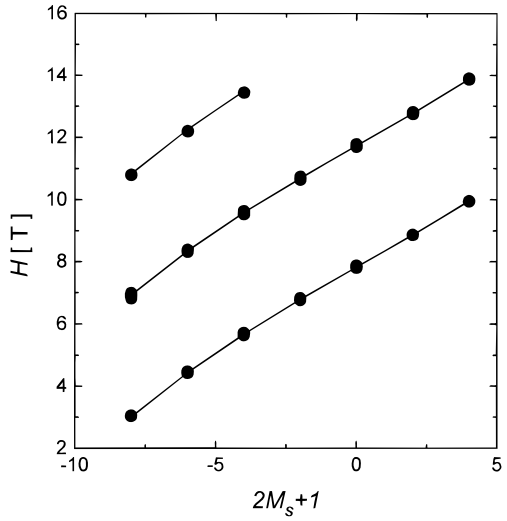

Figure 5. Plot of the resonance fields at which transitions occur plotted versus the value of $(2M_s + 1)$ taken from the pseudo-single-crystal HFEPR data collected for complex **6** at frequencies of 220, 330, and 440 GHz and temperatures of 10 and 30 K. The solid line is a least-squares fitting of these data to eq 5. The fitting parameters are described in the text.

2.00, $D' = -0.57$ cm^{-1} and $B_4^{0'}$=-7.8 $\times$ 10^{-5} cm^{-1}. Since $\theta = 4.49°$, this gives the values of $D = -0.53$ cm^{-1} and $B_4^0 = -7.4 \times 10^{-5}$ cm^{-1}. The fit is plotted in Figure 5. These results may be compared with the recently published HFEPR data on $[Mn_{12}O_{12}(O_2CCH_3)_{16}(H_2O)_4]\cdot 4H_2O\cdot 2HO_2CCH_3$ (**1**), where the reported parameters are $g = 1.93$, $D = -0.46$ cm^{-1} and $B_4^0 = -2.2 \times 10^{-5}$ cm^{-1}.[31]

Magnetization Hysteresis Loops. Recently, magnetization hysteresis loops (M vs H) have been reported[18−20] for $[Mn_{12}O_{12}(O_2CCH_3)_{16}(H_2O)_4]\cdot 4H_2O\cdot 2HO_2CCH_3$ (**1**). Steps were seen at constant intervals of field. Steps were also observed[46] in the hysteresis data for Fe_8 complex **5**. These steps in magnetization are due to a sudden increase in the decay rate of magnetization occurring at specific field values and have been attributed[18−20,46] to field-tuned resonant magnetization tunneling. Complex **1** has appreciable uniaxial magnetic anisotropy caused by a relatively large axial zero-field splitting ($D = -0.46$ cm^{-1}) of the $S = 10$ ground state. There is a potential-energy barrier for an individual molecule of **1** to change the direction of its magnetization from "spin up" to "spin down". In zero field, molecules must either climb over or tunnel through a potential energy barrier of height $D\hat{S}_z^2$. In the presence of a field, the double well is no longer symmetric, and in a positive external field the $M_s = -10$ state becomes the ground state while the $M_s = 10$ state is higher in energy. At high field (30 kOe), the magnetization is saturated and all of the molecules are in the ground $M_s = -10$ state. As the field is decreased, the metastable M_s levels in the left-hand well become closer in energy with the $-M_s$ levels in the right-hand well and at zero field the wells are symmetric. The first step in the hysteresis loop is observed at zero field due to the surge of molecules tunneling between energetically degenerate $-M_s$ and M_s levels. Six additional steps were observed[18−20] when the field was reversed in direction and swept out to −30 kOe. The steps result when the $|S,M_s\rangle$ quantum states in the left-hand-side well become degenerate in energy with the $|S,-M_s+n\rangle$ states in the right-hand-side well (where n = integer), thus allowing molecules to tunnel through the barrier.

In the following sections, evidence of field-tuned magnetization tunneling is given for a third single molecule magnet,

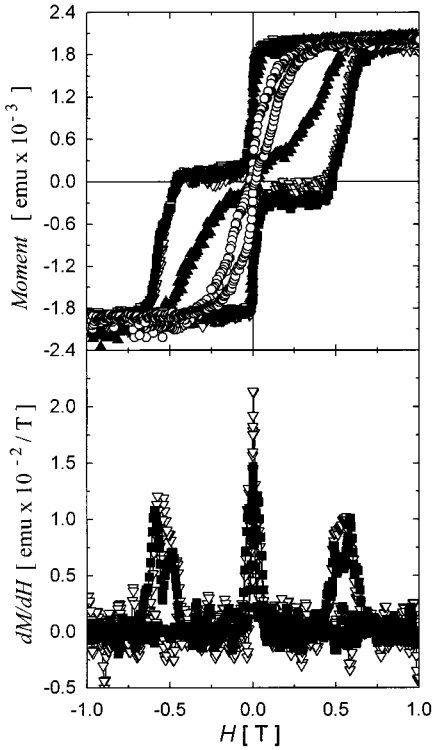

Figure 6. (Top) Magnetic hysteresis loops collected on an oriented single crystal of complex **6** in an eicosane matrix at temperatures of 0.900 (○), 0.706 (▲), 0.530 (▽) and 0.426 K (■). The magnetic moment of the crystal was first saturated in a field of 20 kOe at the desired temperature. Magnetization data were then measured while sweeping the field at a rate of 33 Oe/s from 20 kOe to −20 kOe and back. In the bottom of the figure is a plot of the first derivative of magnetic moment (dM/dH) versus magnetic field. Peaks seen in the first derivative plots correspond to the fields at which steps are seen in the hysteresis plots.

$[Mn_4O_3Cl(O_2CCH_3)_3(dbm)_3]$ (**6**). Resonant magnetization tunneling in complex **6** is of particular interest, because it has a half-integer ground state, $S = {}^9/_2$, and it is appreciably smaller in size than the Mn_{12} complex. Evidence for magnetization tunneling in the Mn_4 complex **6** is presented in the form of hysteresis loops, magnetization decay, and ac susceptibility data.

Magnetization hysteresis data were obtained on a 63 μg platelike single crystal ($\sim 1 \times 1 \times 0.1$ mm) of $[Mn_4O_3Cl(O_2CCH_3)_3(dbm)_3]$ (**6**) at five different temperatures between 0.426 and 2.21 K employing a Faraday magnetometer equipped with a ^{3}He cryostat. The single crystal was oriented in eicosane such that the axial anisotropy axis of the molecule is parallel with the external field (see physical measurements section for details). The sample was cooled to the desired temperature in a field. After saturating the moment ($M_{sat} = 2 \times 10^{-3}$ emu) at 20 kOe, the field was swept down to −20 kOe and then back up to 20 kOe at a rate of 33 Oe/s. Each hysteresis loop took 40 min to measure. At 2.1 K no hysteresis is seen. In the top of Figure 6 is plotted the magnetic moment vs external field H. Hysteresis loops are observed at 0.900 (○), 0.706 (▲), 0.530 (▽) and 0.426 K (■), where four steps are clearly evident in each of these hysteresis loops. The first derivative of the magnetic moment, dM/dH, is plotted versus the external field H in the lower part of Figure 6. At 0.426 K (■), as the field is reduced from 20 kOe a sharp drop in magnetization to 0.2 $\times$ 10^{-3} emu is observed at $H = 0$. When the field is reversed in direction and swept to −20 kOe, another smaller step is seen at −5.4 kOe. Similar steps are also apparent when sweeping the field from −20 kOe to 20 kOe. It is interesting to note that the

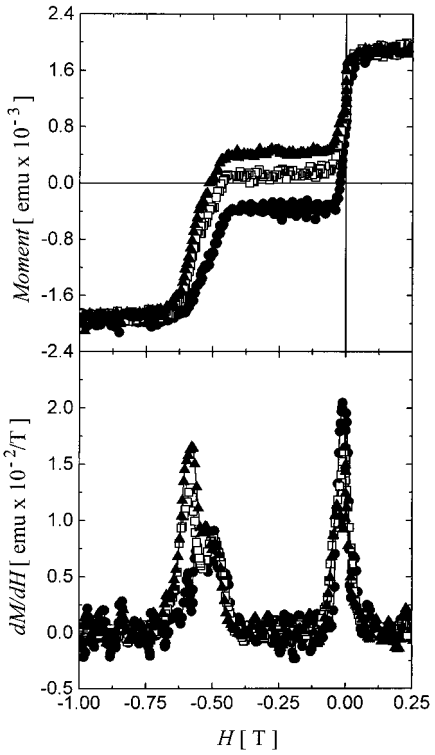

Figure 7. In the upper part of the figure are plotted magnetic moment versus field data for a single oriented crystal of complex **6** in an eicosane matrix at 0.426 K for sweep rates of 66 (▲), 33 (□), or 6.6 Oe/s (●). In the lower part of the figure the first derivative of magnetic moment (d*M*/d*H*) is plotted versus field.

hysteresis loops observed at 0.426 K (■) and 0.530 K (▽) overlap. The small deviation in the 0−5 kOe range on the sweep from −20 kOe to +20 kOe may be due to an artifact in the measurement at 0.426 K. To change the direction of the field, a switch is manually flipped at zero field that changes the polarity of the current. Due to rapid magnetic relaxation at $H = 0$, small variations in the time spent at low fields are seen to have an effect on the subsequent data. The overlap of the two lowest-temperature hysteresis loops (0.426 and 0.530 K) indicates that the relaxation behaviors at these two temperatures are the same. This is not surprising in light of the fact that we have found that below 0.600 K the relaxation rate is independent of temperature (vide infra). At 0.706 K (▲) and 0.900 K (○), only the step seen at zero field is visible. However, the step at $H = 0$ is less steep for the 0.706 and 0.900 K loops than for the other two. This is an indication that the resonant magnetization tunneling is thermally assisted. At the higher temperatures, quantum tunneling may be occurring in the excited states *(i.e.* $-^7/_2 \rightarrow {}^7/_2$, $-^5/_2 \rightarrow {}^5/_2$, ..., etc.).

Experiments were carried out in order to see if the amplitudes of these steps observed at field values of 0, −5.4, and 5.4 kOe are dependent on the sweep rate of the magnetic field. One leg of the hysteresis loop was measured at 0.426 K from 20 kOe to −20 kOe at sweep rates of 66 (▲), 33 (□), and 6.6 Oe/s (●). The resulting moment vs *H* data are plotted in the top of Figure 7. Two observations were made: first, the fields at which the steps occur are independent of sweep rate as seen in the first derivative plots at the bottom of Figure 7; second, as the field is swept at a slower rate the magnetization step is larger at zero field, but smaller at 5.4 kOe.

The above observations of steps on magnetization hysteresis loops and the sweep rate dependence of the step heights can be qualitatively explained at this point. In the experiments described the single crystal was first put in a large field of 20 kOe. In this field the $M_s = -^9/_2$ level (spin aligned with the field) is stabilized considerably in energy relative to the $M_s = {}^9/_2$ level. When the magnetization becomes saturated, all of the Mn_4 molecules populate only the $M_s = -^9/_2$ level. A decrease of the field from 20 kOe to zero changes the energy of the $M_s = -^9/_2$ level such that at zero field the $M_s = -^9/_2$ and $M_s = {}^9/_2$ levels have the same energy. To maintain equilibrium, 50% of the molecules should be in the $M_s = -^9/_2$ level, with the other 50% in the $M_s = {}^9/_2$ level when only these two levels are populated at low temperatures. Classically, if a molecule is to convert from the $M_s = -^9/_2$ level to the $M_s = {}^9/_2$ level it would have to go over the potential energy barrier for reversing the direction of magnetization. This may not be possible at the lowest temperatures. As the field is swept from 20 kOe to zero, then to −20 kOe, the magnetization of the collection of Mn_4 molecules reverses direction. The fact that there is hysteresis is a reflection of a kinetic control of the rate of change of magnetization. A hysteresis loop becomes large, i.e., it has a larger coercivity, at lower temperatures because there is less thermal energy available for a molecule to go over the barrier. The steps seen in the hysteresis loop are due to Mn_4 molecules converting from "spin up" ($M_s = -^9/_2$) to "spin down" ($M_s = {}^9/_2$) by quantum mechanical tunneling. The rate of tunneling becomes appreciable when the energies of two levels on opposite sides of the barrier become equal. Thus, when the field is decreased from 20 kOe to zero, the energies of the $M_s = -^9/_2$ and $^9/_2$ levels become equal and many Mn_4 molecules tunnel from "spin up" to "spin down". At slower and slower rates of sweeping the field more time is spent at zero field and more and more molecules can tunnel. Eventually, if enough time is spent at zero field enough molecules will tunnel so as to give equal populations of molecules in the $M_s = -^9/_2$ and $^9/_2$ levels and the magnetization of the crystal would go to zero.

DC Magnetization Decay Experiments in a Field. The influence of an external dc field on the rate of change of magnetization was examined further. It was of interest to see whether turning on a dc field would increase or decrease the rate of magnetization change. At 0.706 K, dc magnetization decay data were collected at zero field and at −3.034 kOe on the same oriented single crystal of [$Mn_4O_3Cl(O_2CCH_3)_3(dbm)_3$] (**6**). The magnetization of the crystal was first saturated in a 20 kOe field at 0.706 K followed by the reduction of the field to zero or −3.034 kOe at which point magnetization measurements were commenced. In the upper part of Figure 8 magnetic moment vs time data collected at either zero field (■) or −3.034 kOe (○) are plotted. It is clear that the rate of magnetization relaxation is faster when the field is zero, than when it is −3.034 kOe. Thus, the ∼−3 kOe field leads to a misalignment of energy levels and this minimizes resonant magnetization tunneling. The magnetization decay data shown in Figure 8 at a given temperature are not well accommodated by a single-exponential decay curve. We shall return to an analysis of these relaxation data later. The relaxation time at −3.034 kOe is *larger* than that at zero field contrary to classical behavior, which predicts a decrease in relaxation time with increasing field. In the classical limit, as the field is increased the relaxation time of a molecule decreases due to the reduction in activation barrier height. The activation barrier *U* as a function of field *H* is given[32] in eq 6

$$U = U_0\left(1 - \frac{H}{H_0}\right)^2 \tag{6}$$

where U_0 is the magnitude of the classical energy barrier ($D\hat{S}_z^2$)

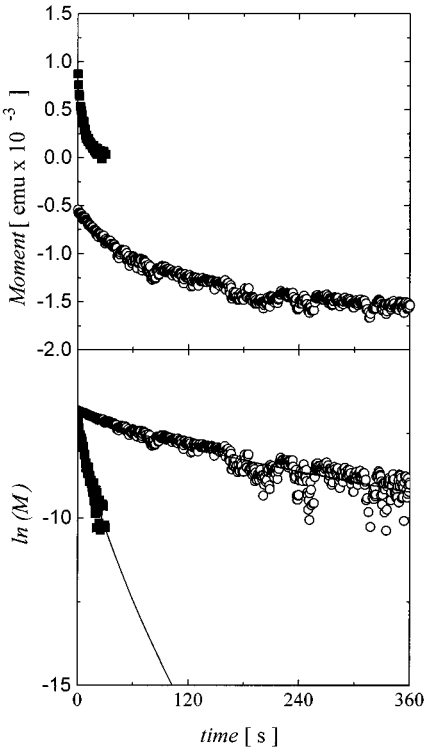

Figure 8. Plot of moment versus time (upper panel) and of natural logarithm of moment vs time (lower panel) collected at either zero field (■) or at −3.034 kOe (○). The magnetization of a single oriented crystal of complex **6** in eicosane matrix was first saturated in a field of 20 kOe at 0.706 K. The field was then reduced either to zero (■) or to −3.034 kOe (○), whereupon magnetization measurements were made. In the lower part of the figure the data are least-squares fit to a stretched single-exponential decay.

in zero field and $H_0 = 2U_0/g\mu_B S$ is the field at which the barrier disappears. When $H_0 \gg H$, then

$$U = U_0\left(1 - \frac{2H}{H_0}\right) \tag{7}$$

However, the decrease in the relaxation rate with the addition of a field of −3.034 kOe is consistent with the presence of field-tuned resonant magnetization tunneling. As can be seen in Figure 6, at zero field a large step is seen in the hysteresis loops due to resonant magnetization tunneling between energetically degenerate $-M_s$ and $+M_s$ levels. At −3.034 kOe, levels are no longer matched up in energy and tunneling is minimized. Therefore, in order for molecules to relax they must climb over the barrier through a thermally activated process and the relaxation time is longer.

Ac Relaxation Data in a Dc Field. Field-tuned magnetization tunneling is also in evidence in the dc field dependence of the ac susceptibility data for $[Mn_4O_3Cl(O_2CCH_3)_3(dbm)_3]$ (**6**). Ac magnetic susceptibility data were collected as a function of temperature with the ac field oscillating at 1000 Hz for different dc fields between 1.0 and −9.0 kOe. A collection of microcrystals oriented in eicosane was used for these experiments. In the upper part of Figure 9, the out-of-phase components of the ac susceptibility χ''_M are plotted vs temperature at five different dc field values in the 0 to −2031 Oe range. To avoid congestion in the figure, the χ''_M data obtained with a dc field in the −5000 to −7013 Oe range are plotted in the lower part of Figure 9. Two observations can be made. First, with increasing field the magnitude of the χ''_M peak decreases. In a

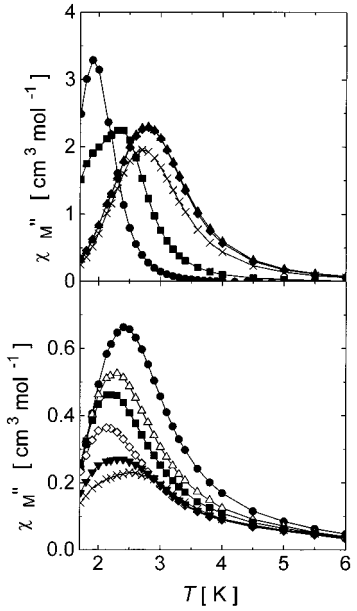

Figure 9. In the upper part of the figure the out-of-phase ac magnetic susceptibility χ''_M is plotted vs temperature as determined for oriented crystals of complex **6** in an eicosane matrix at different settings of an external dc field: 0 (●), −250 (■), −768 (◆), −1000 (▲), and −2031 Oe (×). To avoid congestion, the higher dc field data are plotted in the lower part of the figure for dc field values of −5000 (●), −5400 (△), −5559 (■), −5934 (◇), −6565 (▼), and −7013 Oe (×). For all measurements the amplitude of the 1000 Hz ac field was 1 Oe oscillating.

dc field, the width and height of an out-of-phase χ''_M peak is strongly dependent on spin−lattice relaxation and is not easy to predict. Second, the out-of-phase peaks shift to either higher or lower temperatures at different dc fields. The shift in the temperature at which a peak in χ''_M occurs can be explained in terms of resonant magnetization tunneling. In zero field a sharp out-of-phase peak is observed with a maximum at 1.91 K. Upon increasing the field to −768 Oe, the temperature for the χ''_M peak shifts to *higher* values. The χ''_M vs T data collected at −768 and −1000 Oe overlap and at higher fields the maximum in the χ''_M peak shifts to *lower* temperatures. As the field is changed from −2031 Oe to −5934 Oe, the χ''_M peak continuously shifts to lower temperatures. Between −5934 Oe and −7500 Oe another reversal occurs, shifting the χ''_M peak to higher temperature. In summary, the temperature corresponding to the maximum in the out-of-phase ac peak is plotted versus dc field in Figure 10. If only a thermally activated process was involved, a monotonic drop in temperature should be observed with increasing field as a result of the reduction in activation barrier height as a function of field [eq 7]. However, two dips in temperature are seen, one at zero field and the other at −5.9 kOe. These dips occur at essentially the same fields where steps in the hysteresis loops are observed (i.e. 0, −5.4 kOe). It is at these fields where there is an alignment of energy levels between the two parts of the double well and resonant magnetization occurs. When this occurs the ac peak moves to lower temperatures because tunneling is facilitated, effectively reducing the barrier for changing the direction of the magnetization.

Temperature Dependence of Magnetization Relaxation Rate in Zero Field. Magnetization decay experiments were carried out in the temperature range of 0.700−0.394 K on a Faraday magnetometer. These measurements were performed on a single crystal (63 μg) aligned in eicosane such that the molecule's magnetic anisotropy axis was parallel with the axis

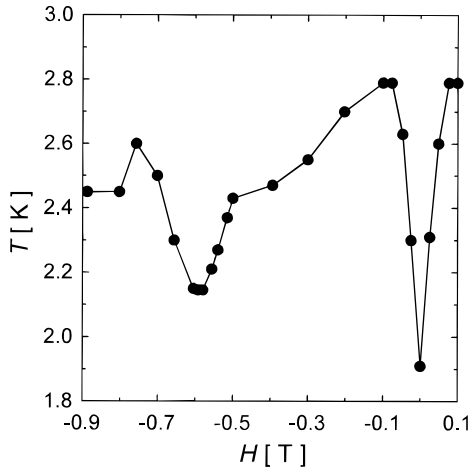

Figure 10. Plot of the temperature for the maximum in the out-of-phase ac susceptibility signal χ''_M versus the magnitude of the dc field for a sample of oriented crystals of complex **6** in an eicosane matrix. The ac field had an amplitude of 1 Oe and was oscillating at 1000 Hz.

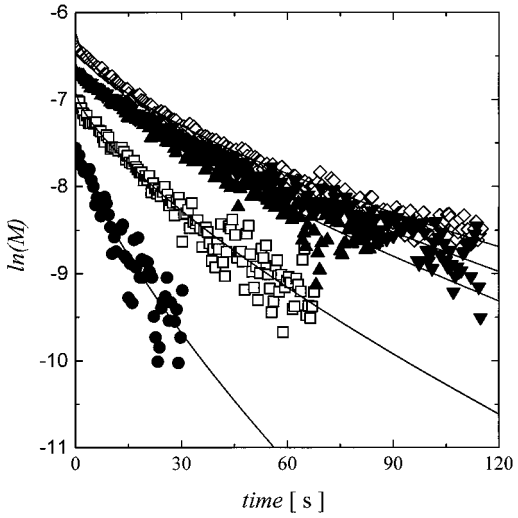

Figure 11. Plots of the natural logarithm of magnetic moment versus time collected on a single crystal of complex **6** oriented in eicosane matrix at temperatures of 0.700 (●), 0.600 (□), 0.506 (▲), 0.458 (◇), and 0.394 K (▼). Saturation of the moment was first achieved at the desired temperature in a field of 20 kOe, followed by reducing the field to zero, and then measurements of the magnetization as a function of time were made. The data were fit to stretched single-exponential decay curves as given in eq 8.

of the external field (details in Experimental Section). Prior to collecting magnetization data, the single crystal was first cooled to the desired temperature in an external field of either 20 or −20 kOe. At |20| kOe, the magnetization of the sample is saturated at a value of $|2| \times 10^{-3}$ emu. The field was then reduced to zero (∼6 min) and the magnetization decay data were recorded over time. Special attention was paid to random oscillatory drifts in magnetization due to the instrument. Two measurements performed at each temperature were found to be essentially superimposable, thus eliminating the possibility that the decay is due to a random instrumental drift in magnetization. Figure 11 gives a plot of the natural logarithm of magnetization versus time collected at 0.700 (●), 0.600 (□), 0.506 (▲), 0.458 (◇), and 0.394 K (▼). At all temperatures, the magnetization goes to zero in less than 2 min. Also, the relaxation curves collected at 0.506, 0.458, and 0.394 K virtually overlap. Attempts to fit the relaxation data at each temperature with a single-exponential decay lead to poor fits. Rather, the relaxation profile is better characterized by a stretched exponential decay,

Table 3. Relaxation Fitting Parameters Resulting from Least-Squares Fitting of Magnetization Decay Data for a Single Aligned Crystal of Complex **6** to a Stretched Exponential Decay

temp [K]	relaxation time τ [s]	ln(M_0)	B
0.394[a]	38	−6.6	0.75
0.458[a]	26	−6.2	0.60
0.506[a]	31	−6.6	0.73
0.600[a]	20	−6.9	0.72
0.700[a]	10	−7.5	0.75
0.394[b]	32	−6.5	0.62
0.426[b]	31	−6.4	0.73
0.458[b]	31	−6.5	0.68
0.506[b]	28	−6.6	0.71
0.600[b]	17	−6.8	0.65
0.706[b]	5.3	−6.9	0.70
0.706[c]	84	−6.6	0.66

[a] The decay in magnetization was measured in zero field after saturating the sample in a field of 20 kOe. [b] The decay in magnetization was measured in zero field after saturating the sample in a field of −20 kOe. [c] The decay in magnetization was measured in a field of −3.034 kOe after saturating the sample in a field of 20 kOe.

$$M = M_0 e^{-(t/\tau)^B} \quad \ln(M) = \ln(M_0) - (t/\tau)^B \qquad (8)$$

which describes a decay that is initially fast and then becomes slower with time. In this equation M_0 is the initial magnetization, τ is the average relaxation time, and B is the width of the distribution. When $B = 1$, the relaxation as a function of time follows a single-exponential decay. The lines in Figure 11 are fits to a stretched single-exponential decay as given in eq 8. The relaxation times (τ) are 38, 26, 31, 20, and 10 s at 0.394, 0.458, 0.506, 0.600, and 0.700 K, respectively. In Table 3 are listed values of ln(M_0), τ, and B at all temperatures measured.

To ensure that the above magnetization relaxations were not due to any instrumental drifts, these measurements were repeated, this time saturating the magnetization in a field of −20 kOe and then reducing the field to zero. The resulting plots of the natural logarithm of magnetization vs time at each temperature are plotted in Figure 12 along with the least-squares fits to eq 8. The resulting relaxation times (τ) are 32, 31, 28, 17, and 5.3 s at 0.394, 0.458, 0.506, 0.600, and 0.700 K, respectively. It can be concluded that the relaxation times are reproducible. Unfortunately, the relaxation times are too short at temperatures above 0.700 K to be characterized by dc magnetization decay experiments.

The reason a stretched exponential is needed to fit each magnetization decay data set is not totally understood. As can be seen in Table 3, the distribution parameter B ranges from 0.60 to 0.75. It is relevant to note that the magnetization relaxation data for the Mn_{12}Ac complex **1** and for the Fe_8 complex **5** also could not be fit to single exponentials. For these two complexes, the initial part of each relaxation data set was left out of the analysis. Even in the single crystal of complex **6** there are likely distributions in the environment about Mn_4 complexes. Defect structures, such as crystallographic dislocations, are present and this leads to a distribution in zero-field interaction parameters D, for example. Such a distribution in D values obviously would produce a distribution in thermodynamic barrier heights ($D\hat{S}_z^2$). It is important to emphasize that the conclusions that are made below from a plot of the logarithm of the relaxation rate versus the inverse absolute temperature are unaffected by using either stretched exponentials or the best single-exponential fit to the data.

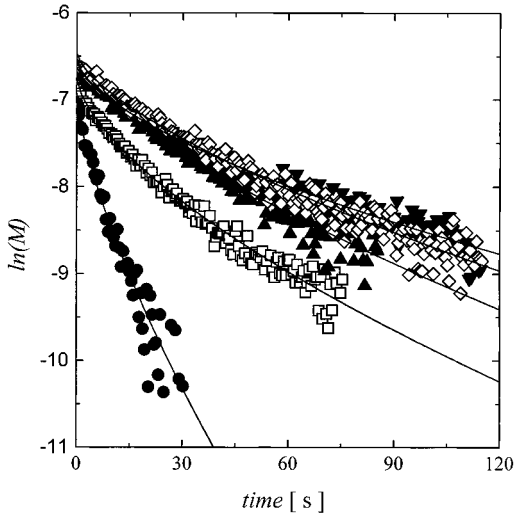

Figure 12. Plots of the natural logarithm of magnetic moment versus time collected on a single crystal of complex **6** oriented in eicosane matrix at temperatures of 0.700 (●), 0.600 (□), 0.506 K (▲), 0.458 (◇), and 0.394 K (▼). Saturation of the moment was first achieved at the desired temperature in a field of −20 kOe, followed by reducing the field to zero, and then measurements of the magnetization as a function of time were made. The lines are a least-squares fit of the data to a stretched single-exponential decay, eq 8.

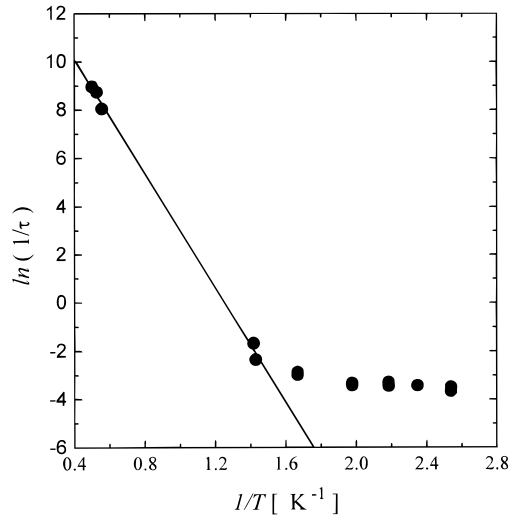

Figure 13. Plot of the natural logarithm of the rate of magnetic moment relaxation ($1/\tau$) versus the inverse of temperature ($1/T$) for $[Mn_4O_3Cl(O_2CCH_3)_3(dbm)_3]$ (**6**). The line is a least-squares fit of the higher temperature data to the Arrhenius equation, eq 9.

The relaxation data for $[Mn_4O_3Cl(O_2CCH_3)_3(dbm)_3]$ (**6**) were examined to see if they could be fit to the Arrhenius eq 9 which describes a thermally activated process:

$$\frac{1}{\tau} = \frac{1}{\tau_0}\exp\left(\frac{-U}{kT}\right) \qquad (9)$$

In this equation U is the activation barrier defined as the magnitude of magnetic anisotropic energy, k is Boltzmann's constant, and the attempt frequency is $1/\tau_0$. Previously, relaxation times were determined for a polycrystalline sample of complex **6** in the 1.8−2 K region with ac magnetic susceptibility measurements.[42] Ac susceptibility data gave relaxation times at 1.8, 1.9, and 2 K of 3.2×10^{-4}, 1.6×10^{-4}, and 1.3×10^{-4} s, respectively. In Figure 13 are plotted the $\ln(1/\tau)$ vs $1/T$ data for temperatures in the range of 0.394−2 K. Clearly there are two different temperature regions, a thermally activated region between 2.0 and 0.700 K and a temperature-independent region between 0.700 and 0.394 K. The relaxation rates measured at temperatures between 2.0 and 0.700 K were least-squares fit to eq 9 to give an activation barrier (U) of 11.8 K and $\tau_0 = 3.6 \times 10^{-7}$ s. Since we are fitting very few points, the error in the parameters U and τ_0 may be large. This is to be compared with the barrier height calculated as $20|D| = 10.6$ $cm^{-1} = 15.2$ K, which is calculated by taking the spin of the ground state as $S = {}^9/_2$, together with the D value obtained by fitting the quasicrystal HFEPR data. With the limited amount of data available the two evaluations of the anisotropy energy are in reasonable agreement. The Arrhenius equation predicts that for an activated process, as the temperature approaches 0 K, the relaxation rate should also approach zero. Interestingly, below 0.6 K, the relaxation rate for complex **6** becomes independent of temperature with $1/\tau = 3.3 \times 10^{-2}$ s^{-1}. This temperature-independent process must correspond to magnetization tunneling between the lowest degenerate levels, the $M_s = {}^9/_2$ and$= -{}^9/_2$ levels.

These results are significant for two reasons. First, $[Mn_4O_3Cl(O_2CCH_3)_3(dbm)_3]$ (**6**) is the third single-molecule magnet that has been reported to display magnetization tunneling. $[Mn_{12}O_{12}(O_2CCH_3)_{16}(H_2O)_4]\cdot 4H_2O\cdot 2HO_2CCH_3$ (**1**) and the Fe_8 complex **5** are the other two molecules reported[14,46] to show magnetization tunneling. The source of magnetic anisotropy in complexes **1** and **5** is zero-field splitting of the $S = 10$ ground state. For Mn_{12}Ac complex **1**,[31] $g_{zz} = 1.93$ and $D = -0.46$ cm^{-1}, and for Fe_8 complex **5**,[45] $g_{zz} = 2.04$ and $D = -0.191$ cm^{-1} as determined by HFEPR measurements. Paulsen *et al.*[14] have reported that the relaxation rate for complex **1** becomes independent of temperature below ∼1.4 K with $1/\tau = 10^{-8}$ s^{-1} or $\tau = 3.2$ years. However, caution must be exercised in interpreting these results since the temperature-independent relaxation time for complex **1** at low temperatures is so long that it is not possible to determine it with any precision, due in part to the existence of drift in the experimental apparatus. More recently, resonant magnetization tunneling has been reported for the Fe_8 complex **5**.[46] A temperature-independent rate was observed below 0.400 K with a tunneling rate of $1/\tau \sim 10^{-4}$ s^{-1}. This relaxation rate corresponds to a relaxation time of $\tau = 2.78$ h.

Magnetization quantum tunneling in $[Mn_4O_3Cl(O_2CCH_3)_3(dbm)_3]$ (**6**) can be explained with the assistance of the potential energy diagram in Figure 14. In zero field, appreciable uniaxial magnetic anisotropy ($D\hat{S}_z^2$) due to the large zero field splitting ($D = -0.53$ cm^{-1}) of the $S = {}^9/_2$ ground-state results in an anisotropy barrier for the flipping of spins of the molecules. Thus, in order for a molecule to flip its spin from "up" in the $M_s = {}^9/_2$ level to "down" in the $M_s = -{}^9/_2$ level the molecule must either climb over the barrier or tunnel through the barrier to the other side. Since in zero field the M_s levels on the left-hand side of the barrier are degenerate in energy with the negative M_s levels on the right-hand side well, resonant magnetization tunneling is facilitated. A similar model has been put forth to explain the origin of magnetization tunneling in complexes **1** and **5**.

The second point of significance associated with the observation of magnetization tunneling for complex **6** centers around the spin of the $S = {}^9/_2$ ground state of this Mn_4 complex. In zero magnetic field, a molecule with a half-integer spin ground state should not be able to quantum mechanically tunnel. This is the essence of Kramers degeneracy. In general, the wave

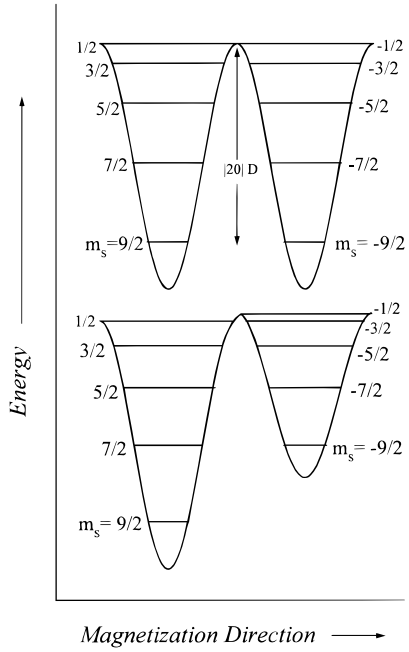

Figure 14. Plot of potential energy vs the magnetization direction for a single molecule with a $S = {}^9/_2$ ground state. In zero applied field (top of figure), axial zero-field splitting ($D\hat{S}_z^2$) splits the $S = {}^9/_2$ state into energetically degenerate, $\pm{}^9/_2$, $\pm{}^7/_2$, $\pm{}^5/_2$, $\pm{}^3/_2$, and $\pm{}^1/_2$ levels. The potential-energy barrier height is $20|D|$ for a thermally activated process where the magnetization of the molecule converts from the "spin up" $M_s = -{}^9/_2$ level to the "spin down" $M_s = {}^9/_2$ level. In a negative field (bottom of figure), the symmetry is broken and the ${}^9/_2$ level becomes the lowest energy state.

function for a molecule is given by eq 10,

$$\psi_n(r,t) = \psi_n(r)\exp(iE_nt/\hbar) \tag{10}$$

where $\psi_n(r)$ is the time-independent part of the wave function for a molecule in its nth electronic state with an energy of E_n. In the absence of a magnetic field there is time reversal symmetry. The energy E_n for a state is given in terms of the spin S of the state. Since $\exp(iS\pi) \neq \exp(-iS\pi)$ when S is a half-integer value, coherent tunneling is not possible. In zero field such a $S = {}^9/_2$ molecule cannot coherently tunnel from the $M_s = -{}^9/_2$ level to the $M_s = {}^9/_2$ level.

However, when the single crystal of the Mn_4 complex **6** is at low temperatures and the external field is decreased from 20 kOe to zero, a large step is seen in the hysteresis loop. There clearly is magnetization tunneling in zero external magnetic field. The origin of this tunneling is very likely the internal magnetic field within the Mn_4 complex due to the nuclear spins. The manganese ($I = {}^5/_2$) and hydrogen ($I = {}^1/_2$) atoms in complex **6** possess nuclear magnetic moments. Together they lead to an internal magnetic field of ~50−100 G. Even though this is a relatively small field, a transverse component of this internal field would be sufficient to lead to magnetization tunneling. There already has been considerable discussion in the literature[48] about the potential effects of an internal field created by nuclear spins on magnetization tunneling in nanomagnets.

Origin of Field-Tuned Magnetization Tunneling. All of the data presented above can be explained in terms of field-tuned resonant magnetization tunneling. The simplest spin Hamiltonian that models this system is given in eq 1. The first term in the Hamiltonian is the Zeeman term and the second is the axial zero-field splitting term. When the field is applied parallel relative to the z axis (easy axis) of the molecule, then the eigenvalues are given as:

$$E = g\mu_B H_z M_s + DM_s^2 \tag{11}$$

This results in a double-well potential energy diagram (Figure 14), where the positive and negative M_s quantum levels are separated by an activation barrier. In zero field, the double well is symmetric and so the M_s levels (spin "down") in the left-hand well are degenerate in energy with the corresponding $-M_s$ levels (spin "up") in the right-hand well. In the presence of a field the symmetry is broken and one well becomes lower in energy compared to the other. In a large positive field, the Mn_4 molecules populate only the $-M_s$ levels. As the field is decreased to zero the double well becomes symmetric and molecules tunnel from the $-M_s$ level to the M_s level. When the field is reversed and swept out to a large negative field (lower part of Figure 14) sharp increases in the relaxation rate are seen as a result of M_s levels matching up in energy with $(-M_s + n)$ levels (where n is an integer). At these fields resonant magnetization tunneling occurs. The field at which the energy of an M_s level becomes degenerate with that of a $(-M_s + n)$ level can be obtained by setting the two energy expressions given by eq 11 equal to one another and solving for H:

$$M_s g\mu_B H + M_s^2 D = (-M_s + n)g\mu_B H + (-M_s + n)^2 D \tag{12}$$

After gathering like terms, it is found that the field at which a M_s level is degenerate in energy with a $(-M_s + n)$ level is given by eq 13:

$$H = \frac{-nD}{g\mu_B} \tag{13}$$

Level matching occurs at a constant interval of field (ΔH) as in eq 14.

$$\Delta H = \frac{D}{g\mu_B} \tag{14}$$

Steps in the hysteresis loops are observed at a field interval of $\Delta H = 5.4$ kOe, which corresponds to $D/g = 0.25$ cm^{-1}. Similar results are seen in the ac susceptibility measurements where ΔH is 5.9 kOe and therefore $D/g = 0.27$ cm^{-1}. This is in very good agreement with the values of D (−0.53 cm^{-1}) and g (1.99) obtained from HFEPR measurements, where $D/g = 0.26$ cm^{-1}. These results confirm that magnetization tunneling *is* occurring at fields corresponding to level matchings.

In the top of Figure 15 the energies are plotted of the various components of the $S = {}^9/_2$ state versus field which shows the fields at which the $+M_s$ levels become energetically degenerate with the $(-M_s + n)$ levels. The ground state is taken as $S = {}^9/_2$ with $D = -0.53$ cm^{-1}. At zero field, five (M_s; $-M_s + n$) level combinations are degenerate in energy, setting up multiple resonances for quantum mechanical tunneling. As n increases, a sequential reduction by 1 in the number of levels matched up at the field crossing occurs. Level matching is predicted at five field values: 0, 5.7, 11.4, 17.1, and 22.8 kOe for positive values of field. However, only two steps in the hysteresis loops are seen. In a thermally activated process, the activation decreases with increasing field and therefore the relaxation rate increases. Observation of quantum tunneling at higher fields is being obscured by the very fast relaxation rates of molecules thermally activated over the barrier. Even at low temperatures (i.e. 0.4−

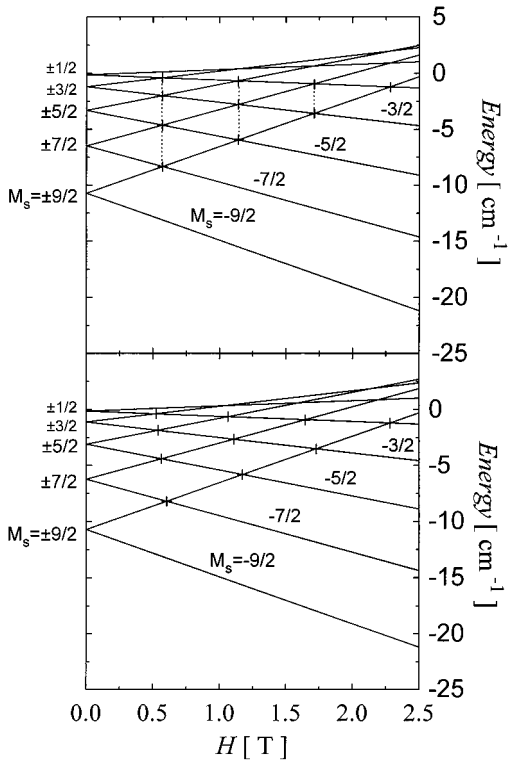

Figure 15. Plot of energy vs field depicting the field values at which M_s levels become energetically degenerate with $(-M_s + n)$ levels for a molecule with a $S = {}^9/_2$ ground state split by axial zero-field splitting with $D = -0.53$ cm^{-1}, $g = 1.998$, and the higher order zero-field splitting term $B_4{}^0$. In the upper part of the figure the higher order term $B_4{}^0$ is zero, while in the lower part of the figure $B_4{}^0$ is -7.29×10^{-5} cm^{-1}.

0.9 K), the relaxation times are on the order of minutes. Perhaps more steps in field could be observed by using a faster technique such as ac susceptibility measurements at lower temperatures.

Small deviations from the above model are expected since the higher order term, $B_4{}^0$ is present in this system. From high-field HFEPR measurements, the quartic term $B_4{}^0$ was found to be -7.29×10^{-5} cm^{-1}. Although small, the $B_4{}^0$ term affects the position at which steps occur in two ways. First, ΔH is no longer a constant and steps are *not* expected to occur at a constant interval of field. Second, at field crossing where $n \neq 0$, multiple level matching is *not* observed. It can be shown that the interval between two states characterized by M_s and $(-M_s + n)$ is

$$\Delta H = \frac{[D - 717.5\mathrm{B}_4{}^0 + 35B_4{}^0(2M_s{}^2 - 4M_s n - 2M_s + 3n^2 + 3n + 1)]}{g\mu_B} \quad (15)$$

The impact of the quartic term $B_4{}^0$ is evident in the bottom of Figure 15, where the energy is plotted as a function of field where $S = {}^9/_2$, $D = -0.53$ cm^{-1}, and $B_4{}^0 = -7.29 \times 10^{-5}$ cm^{-1}. It is observed that multiple levels are no longer matched up at a constant field as in the case when $B_4{}^0 = 0$ (upper part of Figure 15). Rather, the M_s and $(-M_s + n)$ levels match up within a small field range spanning ~900 Oe. At a given value of n, the M_s, $(-M_s + n)$ level matching occurs at higher field for larger values of M_s. For example, at $n = 1$, the $({}^9/_2, -{}^7/_2)$ level crossing occurs at 6.03 kOe while the $({}^3/_2, -{}^1/_2)$ level-crossing occurs at a lower field of 5.21 T. Similar observations are made for the higher n values where for $n = 2$ the field range is 1099 Oe and for $n = 3$ the field range is 824 Oe. Therefore, if quantum tunneling is occurring at multiple levels, the resulting step in the hysteresis loops will be broadened and will be temperature dependent. At lower temperatures the step will become sharper and shift to slightly higher fields. A second point is that $\Delta H_{M_s,-M_s+n}$ is no longer a constant as observed in the case where $B_4{}^0 = 0$ (upper part of Figure 15). In contrast, a difference in ΔH values of 500−900 Oe for $n \neq 0$ is predicted. Experimentally, since only two steps are seen in the hysteresis loops and given the noise, these subtleties in field positions are difficult to discern.

The mechanism by which resonant magnetization tunneling occurs is still under study. Axial zero-field splitting ($D\hat{S}_z{}^2$) does not lead to magnetization tunneling. For magnetization tunneling to occur anisotropy perpendicular (transverse) to the z-axis is required. Some researchers[31] have suggested that tunneling in $[Mn_{12}O_{12}(O_2CCH_3)_{16}(H_2O)_4]\cdot 4H_2O\cdot 2HO_2CCH_3$ (**1**) may be due to a transverse component in the magnetocrystalline anisotropy tensor. Because the Mn_{12}Ac complex **1** has S_4 site symmetry in the crystal, the lowest order transverse zero-field interaction term allowed is the quartic term $B_4{}^4(\hat{S}_+{}^4 + \hat{S}_-{}^4)$. However, only transitions corresponding to $\Delta M_s = \pm 4$ are allowed. Therefore, only every other step in the hysteresis loop would be observed corresponding to when n is an even number. Friedman *et al.*[19b] have suggested that a small transverse magnetic field may be the origin of the magnetization. No steps are prohibited since $\Delta M_s = \pm 1$ are allowed.

In zero applied field there is a 2-fold degeneracy for each state: $M_s = 10$ and -10, $M_s = 9$ and -9, etc. A transverse *internal* magnetic field breaks these 2-fold degeneracies. Garanin[49] has derived an expression for the tunneling splitting due to a transverse field in zero applied field. The transverse field provides a perturbation, $\hat{H}' = b\hat{S}_x = {}^1/_2 b(\hat{S}_+ + \hat{S}_-)$, where b equals $g\mu_B H_{trans}$. The tunnel splitting ΔE_{M_s} of each level is given[49] by eq 16

$$\Delta E_{M_s} = \frac{2D(S + M_s)!}{[(2M_s - 1)!]^2(S - M_s)!}\left(\frac{b}{2D}\right)^{2M_s} \quad (16)$$

The rate of magnetization tunneling between two levels, M_s and $-M_s$, is equal to $\Delta E_{M_s}/h$, where h is Planck's constant, and the tunnel splitting is ΔE_{M_s}. Friedman et al.[30] have calculated the magnetization tunneling rates expected for the Mn_{12}Ac complex **1** in zero external magnetic field in the presence of a small (100 G) transverse internal magnetic field. This small transverse internal field could arise from the nonzero nuclear spins. They calculated a magnetization tunneling rate of 2.2×10^{-45} s^{-1} for the $M_s = -10$ to 10 tunneling. As can be seen in Table 4 the tunneling rate calculated for the Mn_{12}Ac complex **1** increases for higher-energy M_s levels. For example, for the $M_s = -3$ to 3 magnetization tunneling the rate was calculated to be 3.5 s^{-1}.

The calculated tunneling rate for the $M_s = -10$ to 10 conversion of a $S = 10$ molecule due to a 100 G transverse internal magnetic field is very small. The lifetime for this tunneling is longer than the lifetime of the universe. This has led Friedman et al.[30] to suggest that in zero external field the Mn_{12}Ac complex **1** exhibits resonant magnetization tunneling via an Orbach process. In zero external field the Mn_{12} molecules are excited to higher M_s levels via a multiphonon Orbach process. In other words, individual molecules interact with phonons and are excited from the $M_s = -10$ level to the $M_s = -3$ level, for example, where the magnetization tunneling rate

(49) Garanin, D. A. *J. Phys. A: Math. Gen.* **1991**, *24*, L61.

Table 4. Tunneling Rates Calculated Using Eq 16 for $[Mn_{12}O_{12}(O_2CCH_3)_{16}(H_2O)_4]\cdot 4H_2O\cdot 2HO_2CCH_3$ (**1**) and $[Mn_4O_3Cl(O_2CCH_3)_3(dbm)_3]$ (**6**)

M_s	tunneling rates $[s^{-1}]^a$, complex **1**	M_s	tunneling rates $[s^{-1}]^b$, complex **6**	tunneling rates $[s^{-1}]^c$, complex **6**	tunneling rates $[s^{-1}]^d$, complex **6**
1	3.2×10^{8}	0.5	1.4×10^{9}	2.8×10^{10}	1.9×10^{10}
2	1.1×10^{5}	1.5	6.5×10^{5}	5.22×10^{9}	1.6×10^{9}
3	3.5	2.5	7.4	2.4×10^{7}	3.2×10^{6}
4	2.3×10^{-5}	3.5	1.0×10^{-5}	1.3×10^{4}	790
5	4.7×10^{-11}	4.5	2.3×10^{-12}	1.2	0.032
6	3.7×10^{-17}				
7	1.2×10^{-23}				
8	1.8×110^{-30}				
9	1.1×10^{-37}				
10	2.2×10^{-45}				

[a] Tunneling rates calculated for complex **1** assuming $S = 10$, $g = 1.91$, $|D| = 0.41$ cm^{-1}, $B_{trans} = 100$ G. [b] Tunneling rates calculated for complex **6** assuming $S = {}^9/_2$, $g = 2$, $|D| = 0.53$ cm^{-1}, $B_{trans} = 100$ G. [c] Tunneling rates calculated for complex **6** assuming $S = {}^9/_2$, $g = 2$, $|D| = 0.53$ cm^{-1}, $B_{trans} = 2000$ G. [d] Tunneling rates calculated for complex **6** assuming $S = {}^9/_2$, $g = 2$, $|D| = 0.53$ cm^{-1}, $B_{trans} = 1340$ G.

is appreciable. Thus, through an Orbach process a single tunneling channel, such as the $M_s = -3$ to 3 conversion, opens up and this gives the step at zero field in the hysteresis loop. If this is the mechanism for tunneling in the $S = 10$ Mn_{12} complex, then the rate of magnetization tunneling would be expected to follow an Arrhenius-like dependence on temperature. A temperature-independent rate of tunneling between the $M_s = -10$ and $M_s = 10$ levels would *not* be seen, for the rate of this tunneling process is too low to be practically detected. The reported temperature-independent rate of tunneling for Mn_{12}-Ac complex **1** is controversial.

For the Mn_4 complex **6** we have determined a temperature-independent magnetization tunneling rate of 3.2×10^{-2} s^{-1} in the 0.394−0.700 K range. This must be due to ground-state tunneling between the $M_s = -{}^9/_2$ and ${}^9/_2$ levels of this $S = {}^9/_2$ molecule. As can be seen in eq 16 the tunnel splitting ΔE, and therefore the rate of tunneling, due to a transverse field is quite dependent on the M_s values of the states involved in the tunneling. We have employed eq 16 to calculate the $M_s = -{}^9/_2$ to ${}^9/_2$ tunneling rate for a $S = {}^9/_2$ molecule in zero external field with a transverse internal field of 100 G (see Table 4). The $M_s = -{}^9/_2$ to ${}^9/_2$ tunneling rate is calculated to be 2.3×10^{-12} s^{-1} for $H_x = 100$ G. For an internal transverse field of $H_x = 2000$ G we calculate a $M_s = -{}^9/_2$ to ${}^9/_2$ tunneling rate of 1.2 s^{-1} (Table 4). The observed temperature-independent tunneling rate for Mn_4 complex **6** of 3.2×10^{-2} s^{-1} corresponds to a transverse internal field of 1340 G. Such an internal magnetic field could arise from the nonzero nuclear spins of the Mn and H atoms in complex **6**; however, 1340 G seems to be on the high side of what would be expected from the nuclear spins. Each Mn atom has a nuclear spin of $I = {}^5/_2$ and each H atom $I = {}^1/_2$. Dipolar interactions due to the spins of neighboring $S = {}^9/_2$ molecules in the crystals could also add to the field created by the nuclear spins.

In the temperature range of 0.40−0.70 K there are less than 0.1% of the Mn_4 molecules in the $M_s = \pm{}^7/_2$ levels in zero external magnetic field. At 2.0 K some 4.7% of the Mn_4 molecules are in the $M_s = \pm{}^7/_2$ levels with the remainder in the $M_s = \pm{}^9/_2$ levels. It is expected that the rate of magnetization tunneling for the $M_s = -{}^7/_2$ to ${}^7/_2$ conversion would be several orders of magnitude greater than the rate of the $M_s = -{}^9/_2$ to ${}^9/_2$ tunneling. Thus, the overall temperature dependence of rate of magnetization relaxation shown in Figure 13 for complex **6** in the 0.4−2.0 K range could be due to magnetization tunneling. The 4.73% population of molecules in the $|M_s| = {}^7/_2$ level at 2.0 K leads to the apparent Arrhenius-like increase in rate of relaxation. The theoretical model used to calculate the tunneling rates given in Table 4 is only approximate. The internal field created by the nuclear spins could well not be homogeneous.

Concluding Comments

The nature of the single-molecule magnet $[Mn_4O_3Cl(O_2CCH_3)_3(dbm)_3]$ (**6**) was probed with several techniques. High-field EPR (218−437 GHz) data clearly show that complex **6** has a $S = {}^9/_2$ ground state experiencing axial zero-field splitting ($D\hat{S}_z^2$) where $D = -0.53$ cm^{-1} and a longitudinal quartic zero-field splitting with $B_4^0 = -7.4 \times 10^{-5}$ cm^{-1}. Hysteresis is seen in the plots of magnetization versus external magnetic field obtained for a 63 μg crystal in the 0.900−0.426 K region. In this low-temperature region each Mn_4 molecule can be magnetized. It is known that this is a single-molecule response because in a previous ac susceptibility study[42] it was shown that complex **6** shows slow magnetization relaxation when the complex is frozen in a dilute solution.

Evidence for field-tuned resonant magnetization tunneling was found in both the dc magnetization hysteresis loops and the ac susceptibility data for complex **6**. The possibility of magnetization tunneling has been studied for many years as it may occur in domain wall movement in macroscopic magnets, magnetic bubbles, and single-domain nanomagnets. Steps are seen in the hysteresis loop for complex **6**. When the energy levels ($M_s = -{}^9/_2, -{}^7/_2, -{}^5/_2, -{}^3/_2, -{}^1/_2$) in one-half of the potential-energy double well become equienergetic with levels ($M_s = {}^9/_2, {}^7/_2, {}^5/_2, {}^3/_2, {}^1/_2$) in the other half of the double well, quantum mechanical tunneling occurs in the direction of magnetization for an individual molecule. This resonant effect is also seen in the ac susceptibility data. The temperature at which the out-of-phase ac signal χ''_M is seen is influenced by an external dc field. At the dc fields where resonant tunneling is expected, the χ''_M peak shifts to a lower temperature.

Interesting observations were made in the study of the relaxation of the magnetization of complex **6** in zero field. An oriented single crystal is first saturated in its magnetization in a large field and then the field is decreased to zero and the time decay of the magnetization was followed. First, it is interesting to see that a molecule with a half-integer spin ground state ($S = {}^9/_2$) can exhibit magnetization tunneling in zero external field. Tunneling is in evidence in the temperature-independent magnetization relaxation rate below ∼0.6 K. A Kramers degenerate molecule such as complex **6** should not be able to coherently tunnel from the $M_s = -{}^9/_2$ to the $M_s = {}^9/_2$ level. There must be a large enough transverse internal magnetic field to facilitate the tunneling. This internal field likely arises from the nuclear spins present in the molecule.

Single-molecule magnets now include the present Mn_4 complex **6**, one Fe_8 complex,[45] and several Mn_{12} complexes.[5−38] These molecules range in size from ∼10 to ∼20 Å in diameter. It will be instructive to identify larger molecules with ground states with an even higher spin than $S = 10$ and/or greater magnetic anisotropies. The goal is to increase the blocking temperature, below which an individual molecule can be magnetized. These single-molecule magnets possess many advantages over nanoscale magnets obtained by fragmenting large magnetic particles. The single-molecule magnets have a defined size, not a distribution in sizes. Single-molecule magnets are in general soluble in common organic solvents. Potentially, Langmuir−Blodgett films could be fabricated from

them. Also, by nature single-molecule magnets permit more facile engineering of shape, size, spin, etc., than do fragmented nanomagnets.

Acknowledgment. This work was supported by the National Science Foundation (G.C. and D.N.H.), the Department of Energy under Grant No. DE-FG03-86ER-45230M.B.M., and the NHMFL Science Program and NHMFL User Program. The ac magnetic susceptibility measurements were performed with a MPMS2 SQUID magnetometer provided by the Center for Interface and Material Science, funded by the W. M. Keck Foundation. The authors benefited from discussions with M. Sarachik and J. Friedman.

Supporting Information Available: High-field EPR spectrum for a powdered sample of complex **6** (1 page, print/PDF). See any current masthead page for ordering information and Web access instructions.

JA974241R